Editors' Suggestion

Triplet-Polaron-Annihilation-Induced Degradation of Organic Light-Emitting Diodes Based on Thermally Activated Delayed Fluorescence

Bas van der Zee, Yungui Li, Gert-Jan A.H. Wetzelaer, and Paul W.M. Blom[*]
Max Planck Institute for Polymer Research, Ackermannweg 10, 55128 Mainz, Germany

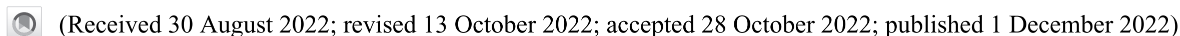

(Received 30 August 2022; revised 13 October 2022; accepted 28 October 2022; published 1 December 2022)

Insufficient operational lifetime continues to be one of the most challenging problems for organic light-emitting diodes (OLEDs) based on thermally activated delayed fluorescence (TADF). Here, we study the degradation of single-layer OLEDs based on the TADF emitter 9,10-bis[4-(9*H*-carbazol-9-yl)-2,6-dimethylphenyl]-9,10-diboraanthracene. After quantitatively describing the current-voltage (J-V) and efficiency curves after electrical driving, we use a numerical model to reproduce the voltage increase and light decrease during degradation. We demonstrate that the fundamental mechanism behind OLED degradation is electron- and hole-trap formation due to triplet-polaron annihilation, the same as that reported for polymer light-emitting diodes. Other mechanisms, such as triplet-triplet annihilation and singlet-triplet annihilation, do not match experimental data. Understanding of the degradation mechanism allows us to predict how a broader emission zone in a thicker single-layer TADF OLED affects its lifetime, resulting in an improved stability with a T_{80} lifetime of 1050 h at an initial luminance of 1000 cd m^{-2}.

DOI: 10.1103/PhysRevApplied.18.064002

I. INTRODUCTION

A longstanding problem for organic light-emitting diodes (OLEDs) is degradation of the emitter under electrical operation. Especially for blue emitters, where exciton energies are inherently high, device stability continues to be a significant issue [1–4]. In the last decade, thermally activated delayed fluorescence (TADF) emitters have attracted much scientific attention due to their promise of delivering 100% internal quantum efficiency without incorporating heavy-metal components [5–7]. TADF materials possess a small singlet-triplet splitting on the order of milli-electron volts, comparable to the thermal energy at room temperature, allowing for fast reverse intersystem crossing (RISC) from the triplet to the singlet state. Although great progress has been made with regard to the external quantum efficiency (EQE) of TADF OLEDs [8–12], insufficient lifetime still greatly hinders the commercialization of this otherwise promising class of emitters [13,14]. To extend the lifetime, a quantitative understanding of the mechanisms behind the operational degradation of TADF OLEDs is indispensable.

*blom@mpip-mainz.mpg.de

Published by the American Physical Society under the terms of the Creative Commons Attribution 4.0 International license. Further distribution of this work must maintain attribution to the author(s) and the published article's title, journal citation, and DOI. Open access publication funded by the Max Planck Society.

Typically, efficient TADF OLEDs employ a multilayer structure, which complicates a quantitative degradation analysis. In such multilayered device architectures, several layers of different molecules aid in the transport, injection, and blocking of charges and/or excitons. This design introduces many unknown variables, such as the transport properties of the individual layers as well as energy barriers at interfaces. Charge-injecting and -transporting layers are reported to influence degradation in a variety of ways, for example, through the accumulation of charges at an interface [15–17] or via their triplet energy levels [18]. If present, interfacial- and injection-related degradation happens in parallel with degradation of the emitter in the bulk, but a loss in charge injection during degradation cannot fully account for complete device degradation [19]. The common practice of doping a TADF emitter in a host further complicates the interpretation of degradation characteristics, as the choice of host or amount of doping also impacts on the device lifetime [20–23]. To obtain a quantitative picture, interpretation of degradation data would strongly benefit from a simple device structure, as found in fluorescent polymer light-emitting diodes (PLEDs), for example, where the emitter layer simply sits between two metallic electrodes of different work function. Moreover, fluorescent materials are simpler than TADF materials, in terms of photophysics, making degradation studies on PLEDs a suitable reference.

Modeling of degraded PLEDs reveals that, under a constant driving current, both the typical degradation characteristics of a voltage increase and a decrease of the

light output during degradation could be linked to the formation of hole traps [24], as already suggested earlier [25]. In the yellow-emitting polymer superyellow poly(*p*-phenylene vinylene) (SY PPV), the dynamics of trap formation reveal that the interaction between excitons and polarons is responsible for the creation of these degradation traps [26]. The exciton-polaron interaction correctly predicts the scaling of the formed hole-trap density, P_t, with stress time: initially, when the amount of free holes (p) is still larger than P_t, the amount of hole traps exhibits a linear increase with time, combined with a scaling of the aging current density (J_{age}) of ${J_{\text{age}}}^{3/2}$. Subsequently, at later times, when $P_t > p$, the hole-trap formation follows a square-root dependence with stress time, in combination with a linear dependence on J_{age}. In addition, a similar scaling on stress time and J_{age} are found in the orange–red-emitting polymer poly[2-methoxy-5-(2′-ethyl-hexyloxy)-1,4-phenylenevinylene]. This study further confirms that, from the two excitonic species, triplet excitons are the ones responsible for the interaction with charges to form traps [27], as suggested before [28]. Transient photoluminescence experiments reveal that singlet excitons recombine within about 1–2 ns [29], whereas intrinsic triplet lifetimes can extend up to 100 μs [30]. As a result, the steady-state population of triplet excitons can exceed the singlet population by up to 5 orders of magnitude. Additionally, the electrical generation ratio of 1:3 for singlets to triplets further enhances the steady-state population of triplet excitons, as compared to singlet excitons, explaining the experimentally observed detrimental effects of triplet excitons on PLED lifetime.

In contrast to PLEDs, the main mechanism behind TADF OLED degradation is still controversial. Several strategies to enhance the lifetime of TADF OLEDs have been proposed, often revolving around device or molecular design [3,21,31–34], but the underlying causes of degradation are rarely quantitatively addressed. The most commonly cited mechanisms that lead to TADF OLED degradation are triplet-triplet annihilation (TTA) and triplet-polaron annihilation (TPA) or a combination of both [35–40]. In a recent study, using luminescence-quenching measurements, TPA was identified as a major source of degradation in TADF OLEDs [39]. Furthermore, the various degradation mechanisms in TADF OLEDs are quantitatively addressed using kinetic Monte Carlo simulations [41]. We note that both studies are carried out on multilayered OLED structures. It should also be mentioned that device deterioration due to extrinsic effects like those of oxygen or water can be easily circumvented by proper encapsulation or by working in a controlled inert environment, such as a glovebox [19,35,42,43]. To further clarify the degradation mechanism, we study the degradation of *single-layer* TADF OLEDs based on the model emitter 9,10-bis(4-(9*H*-carbazol-9-yl)-2,6-dimethylphenyl)-9,10-diboraanthracene (CzDBA) [44]. After modeling of the undegraded CzDBA OLEDs with a numerical drift-diffusion simulator, from which it is known that TTA is the dominant roll-off mechanism [45,46], we quantitatively explain the current-voltage (*J*-*V*) and efficiency curves after degradation. Due to balanced transport, degraded OLED data are consistent with the formation of both hole and electron traps. The scaling of these traps with time and aging current are consistent with TPA as a trap-formation mechanism. Here, a polaron absorbs the energy of a triplet exciton, thereby promoting the polaron to a higher excited state, whereas the triplet is demoted to the ground state. The energetic polaron then has the ability to break specific bonds in the molecule, fragmenting it. The fragmented products are reported to react further to form traps [47]. Other trap-formation mechanisms, such as TTA and singlet-triplet annihilation (STA), cannot reproduce the experimental characteristics of the degraded OLEDs. Moreover, the interaction coefficient for TPA, leading to degradation traps, is found to be almost the same as the coefficient found in PLEDs. Following the predictions of the degradation model, we experimentally confirm that, increasing the OLED thickness results in reduced triplet-polaron interactions, increasing the T_{80} lifetime up to 1050 h at an initial luminance of 1000 cd/m^2.

II. RESULTS AND DISCUSSION

A. Modeling undegraded CzDBA OLEDs

The device structure of the single-layer CzDBA OLED device is presented in Fig. 1(a). In this device, a neat film of the TADF emitter CzDBA is sandwiched between two electrodes, without charge-transport or blocking layers. Ohmic charge injection is enabled by tunneling interlayers [48], while balanced bipolar transport is facilitated by the low trap density in this material [49], as a consequence of the highest occupied molecular orbital (HOMO) and lowest unoccupied molecular orbital (LUMO) values (−5.93 and −3.45 eV, respectively) being inside the “trap-free window” [50]. Furthermore, the photoluminescence quantum yield in a neat film is over 90% [44], indicative of minor nonradiative losses, such as self-quenching, even in the absence of a host. These factors contribute to a high EQE of 19% at 500 cd A^{-1} for single-layer CzDBA OLEDs [51], making them a suitable model system with which to study the degradation of TADF OLEDs. As a starting point, we use a recently developed device model describing the *J*-*V* and EQE of a CzDBA OLED before degradation [46]. We briefly revisit this model, since it forms the basis for our degradation model. In the drift-diffusion simulator, the current continuity and Poison equations for both charge-carrier species are solved as a function of position on a one-dimensional grid of 1000 points, spread out over the device thickness. The density- and field-dependent mobility is calculated locally using the extended Gaussian disorder model parametrization [52].

To minimize the amount of unknown input parameters, single-carrier devices are used to provide information on the mobility parameters for electrons and holes separately, before being integrated in the OLED modeling [53–55]. Furthermore, the device model also includes the exciton dynamics appropriate for TADF emitters, including intersystem crossing rate, reverse intersystem crossing rate, and exciton annihilation rate coefficient. With this extension, the J-V and EQE-V characteristics of undegraded CzDBA OLEDs are well described [46]. All simulation parameters, including the ones determined from single-carrier devices, can be found in Tables S1 and S2 within the Supplemental Material [59]. The efficiency roll-off is governed by TTA with a rate constant, k_{TTA}, of around 1×10^{-17} m^3 s^{-1}. Furthermore, the observed fast increase of efficiency with voltage, typically originating from competition between Shockley-Read-Hall (SRH) and Langevin-type recombination [56], can be explained by assuming that the small amount of trap states observed in single-carrier devices are emissive [46]. Although the precise origin of these light-emitting traps (LETs) is still under investigation, we speculate that they might originate from aggregated CzDBA molecules [46]. This is in line with publications reporting that carbazole moieties have the tendency to dimerize [57,58]. An aggregated state would still be radiative, since the molecule is intact, but it could possess slightly lower energy levels that would show up as an electrical trap in single-carrier and OLED devices. Similar to the earlier reported results [46], also the undegraded OLEDs used in the present study show a fast initial increase in efficiency above the built-in voltage (V_{BI}), as shown in Fig. 1(b) (black symbols); this is one of the fingerprints of emissive

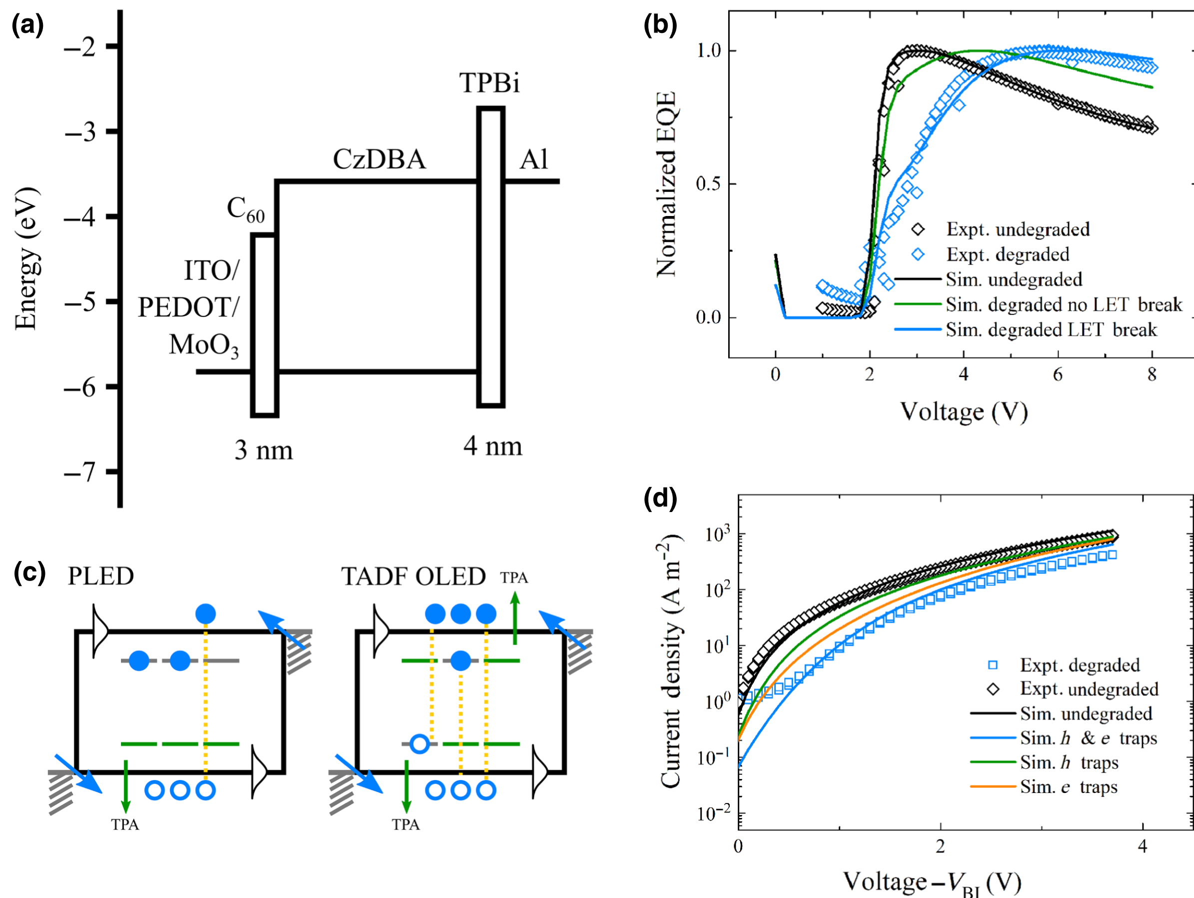

FIG. 1. Device structure, energy diagram, and electrical characteristics of pristine and degraded CzDBA OLEDs. (a) Device structure and energy diagram of CzDBA OLEDs. (b) Normalized experimental (Expt.) EQE as a function of voltage for an OLED with a 300-nm CzDBA layer, accompanied by simulations (Sim.) that show the effect of light-emitting traps (LETs) becoming nonradiative after degradation. (c) Schematic representation of the TPA process in a PLED (left) and TADF OLED (right). Blue solid and empty circles represent holes and electrons, respectively, which are residing either in the HOMO or LUMO (indicated with a Gaussian DOS) or in the trap states before degradation (gray energy levels). Injection is represented by the blue arrows and recombination by the yellow dotted lines. TPA generates the trap states during degradation, which are indicated by the green energy levels. (d) J-V characteristics (corrected for V_{BI}) of a 140-nm CzDBA OLED both undegraded and degraded (symbols) accompanied by simulations (lines).

trap states. Together with the inclusion of TTA, the voltage dependence of the EQE of a 300-nm TADF OLED is quantitatively well described [Fig. 1(b), black line].

B. Trap-formation mechanism in degraded CzDBA OLEDs

A fundamental question is whether the conclusions from degradation studies on PLEDs, namely, hole-trap formation by triplet-polaron annihilation, also apply to TADF OLEDs. When comparing the voltage increase (ΔV) of PLEDs and TADF OLEDs (Fig. S1 within the Supplemental Material [59]), we observe that they display different behavior: whereas PLEDs exhibit a fast initial voltage increase, which slows down over time, TADF OLEDs have, in contrast, a very weak voltage increase in the first few hours, followed by a sharp rise at a certain point in time. One fundamental difference between a SY PPV PLED and a CzDBA OLED is that, in pristine SY PPV, the hole current is several orders of magnitude higher than the electron current, since electron traps are already present with a density of around 1–3 $\times 10^{23}$ m^{-3} before degradation [55]. As schematically indicated in Fig. 1(c) (left), the free-electron concentration is strongly reduced, since most electrons reside in a trap. For CzDBA, both the electron and hole currents are nearly trap free, meaning that the concentration of free electrons and holes is much larger and nearly equal. Trap formation originating from the interaction between free charge carriers and triplet excitons in both materials have significantly different effects on the device performance during degradation. In a PLED, due to the much higher concentration of holes than electrons in a pristine device, mainly hole traps would be formed in the first place. The low concentration of free electrons would strongly limit the formation of electron traps. Consequently, the small amount of electron traps generated during aging is negligible compared to the extrinsic electron traps already present in a pristine device. The dominance of hole-trap generation during PLED degradation is also found experimentally [26]. In contrast, in CzDBA, electron- and hole-trap formation is expected to be equally strong, as schematically indicated in Fig. 1(c) (right). The formation of both electron and hole traps can be confirmed by modeling of the J-V characteristics of a CzDBA OLED after degradation. As shown in Fig. 1(d), good agreement between the experimental and modeled J-V characteristics of a 140-nm degraded CzDBA OLED is only obtained when both hole and electron traps are present. To illustrate the effect of electron and hole trapping on the OLED current, we consider the effect of homogeneously distributed hole *and* electron traps in the CzDBA layer with similar concentrations of 1.2 $\times 10^{23}$ m^{-3}, respectively [see Fig. 1(d), blue line]. For comparison, merely hole [Fig. 1(d), green line] or electron traps [Fig. 1(d), orange line] with a density of 2.4 $\times 10^{23}$ m^{-3} cannot model the J-V curves after degradation. When considering only the effect of a single type of traps (either hole or electron traps), the modeled current density is comparable to the pristine device, which is higher than the experimentally aged one. This can be explained by the fact that both electron and hole transport are nearly trap free in the pristine device: trapping of just one type of carrier does not sufficiently impact the current density, as the other trap-free charge carrier quickly dominates the total current. Therefore, trapping of both electrons and holes is required to explain the degraded J-V, which is thus a consequence of the balanced bipolar transport. The fact that the formation of traps correlates with the presence of free polarons is a first indication that degradation is governed by TPA.

A second fundamental difference between a SY PPV PLED and CzDBA OLED is that in the PLED light emission solely comes from bimolecular Langevin recombination between free electrons and holes. Trap-assisted recombination via extrinsic traps present in pristine devices is of a nonradiative nature [24]. In contrast, trap-assisted recombination from the low amount of traps present in unaged CzDBA OLEDs is radiative, dominating the light emission at low voltages [46]. For degradation processes that involve excitons, such as TPA, result in the breaking of chemical bonds [47], the LETs will also be destroyed and converted into nonradiative degradation traps. Here, we have to take into account that the number of LETs is limited ($\sim 10^{22}$ m^{-3}).

We include the conversion of a LET into a nonradiative trap in our model when calculating the SRH recombination (R_{SRH}). Initially, in the undegraded state, all traps are emissive, resulting in a high internal quantum efficiency [46]. The trap density, N_{t0}, is obtained from the analysis of CzDBA electron- and hole-only devices. We note that N_{t0} is time and position independent. During degradation, the radiative recombination of LETs (R_{LET}) is reduced by the density of LETs that are converted into nonradiative dark traps (N_{DT}), which grows over time during the degradation experiment:

$$R_{\mathrm{LET}}[x,t] = R_{\mathrm{SRH}_0}[x] - \frac{N_{\mathrm{DT}}[x,t]}{N_{t0}} R_{\mathrm{SRH_0}}[x]. \tag{1}$$

Here, $N_{\mathrm{DT}}[x,t]/N_{t0}$ represents the local fraction of traps that are converted from radiative into nonradiative, whereas $1 - N_{\mathrm{DT}}[x,t]/N_{t0}$ is the local fraction of traps that still emit light. R_{SRH_0} represents the initial SRH recombination rate when all traps are still emissive in the undegraded state. Quantities with $[x]$ are taken as position-dependent quantities and $[t]$ as time-dependent quantities. We note that $R_{\mathrm{SRH}_0}[x]$ depends on position, since the densities of free and trapped electrons and holes are position dependent. At the moment that all initially emissive traps, N_{t0}, are converted into dark traps, N_{DT}, Eq. (1) ensures that the contribution of the LETs to the total light output of

the OLED goes to zero. By decreasing the LET recombination with traps obtained from EQE-V, as shown in Fig. 1(c), good agreement between modeling and experimental results can be reached. If all LETs remain intact upon degradation, the modeled efficiency rises too fast (green line), due to (emissive) trap-assisted recombination being dominant at low voltages.

C. Extracting the trap-formation mechanism

As a next step, the voltage and light output versus aging time under current stress are discussed. During the aging tests, the OLEDs are kept at a constant current density, the aging current, while simultaneously the voltage and light output are monitored. To extract the trap-formation mechanism during degradation, we model the voltage increase with the same drift-diffusion approach as that explained above. For an accurate description, it is important to take the formation of both hole and electron traps, as well as the breaking of LETs, into account, and we now outline how this is done for the degradation simulations. In our previous study on the degradation of PLEDs [26], it was assumed that traps generated during degradation would be homogeneously distributed over the active layer. With this assumption, the voltage increase in time can be modeled and described as an increase of formed traps over time. From the observed dynamics of trap formation, it is then concluded that hole-trap formation via TPA is the dominant mechanism [26]. As a refinement, in the present study, both hole and electron traps generated during ageing are now modeled as a function of position. This is rationalized by the nonuniform distribution of charge-carrier and exciton densities throughout the emissive layer in working OLEDs. In this way, for every degradation mechanism, we can model the voltage increase during aging and compare it with experimental results. The modeled voltage versus time is therefore dependent on different models, i.e., different physical mechanisms, to simulate trap formation.

As a first step, we take the local product of charge carriers and triplet excitons to simulate local trap formation via TPA. The hole-trap density (P_t in m^{-3}) (in the case of TPA) for a given time step (t_{step}) is then given by

$$P_t[x] = \kappa p[x]T[x]t_{\mathrm{step}}, \tag{2}$$

with κ (in $\mathrm{m}^3\,\mathrm{s}^{-1}$) as the interaction parameter between the triplet density T (in m^{-3}) and the hole density p (in m^{-3}). An analogous equation is used for electrons with the same value of κ. All quantities that are considered position dependent inside the device are denoted by $[x]$. The interaction coefficient, κ, in Eq. (2) controls the trap-formation rate, which can be treated as a fitting parameter for different experimental aging currents. We note that the assumption of using an equal value of κ for electrons and holes is supported by the fact that we need (nearly) equal amounts of electron and hole traps to be formed after degradation to describe the J-V characteristics of degraded OLEDs, as shown in Fig. 1(b). If the κ values strongly deviate, meaning either electron or hole traps are preferentially formed, the current will be dominated by the nearly trap-free transport of the unaffected carrier, which does not match the experiment. To limit the number of fit parameters, we find it reasonable to assume that $\kappa_p = \kappa_n$ can be used as a first approximation, although we cannot rule out the possibility that they might slightly differ in reality. Furthermore, we also take into account that triplets quenched via TPA to form a degradation trap or break a LET do not participate in the efficiency roll-off through TTA. For alternative degradation mechanisms, such as TTA or STA, $p[x]$ in Eq. (2) is replaced by $T[x]$ or $S[x]$ respectively.

We now turn our attention to the destruction of LETs during degradation. We note that there are two degradation processes taking place that affect the efficiency of the OLED. In one process, similar to a PLED, a free carrier absorbs the energy of a triplet exciton formed by Langevin recombination, leading to the formation of new dark degradation traps by fragmentation of the CzDBA molecules. Next to this, LETs consisting of aggregated or dimerized species of the CzDBA molecules are converted into dark traps by breaking of their chemical bonds via the interaction of triplets residing on these species with free carriers.

The respective trap-formation rates of each process depend on the ratio of the recombination rate of LETs (R_{LET}) versus the normal Langevin recombination rate (R_{Lan}). This ratio represents the proportion of triplet excitons residing on a trap versus regular "free" triplet excitons. The drift-diffusion simulations can be used to model the recombination strength at the sites of emissive traps via SRH and bimolecular Langevin recombination, from which we define the ratio of the emissive SRH recombination rate via LETs (R_{LET}) to the total recombination rate as $\alpha = R_{\mathrm{LET}}/(R_{\mathrm{LET}} + R_{\mathrm{Lan}})$. We then scale the formed trap density for each time step [Eq. (2)] such that αP_t destroys LETs, whereas $(1-\alpha)P_t$ is the amount of "regular" degradation traps created. Over time, the broken LETs reduce the emissive SRH recombination, according to Eq. (1).

After explaining the basic idea of different models for describing trap generation, we now simulate trap formation via the mechanism of TPA. The calculated voltage rise as a function of aging time is influenced by the value of κ and the trap depth of the degradation traps. Figure S2(a) within the Supplemental Material shows the interplay between the two [59], where it becomes clear that greater trap depths cause a larger voltage increase for the same interaction coefficient. In Fig. S2(b) within the Supplemental Material [59], we see that the different trap depths have no significant influence on the light output *for the same value of* κ. However, the overshooting voltage should be corrected by lowering κ until it fits the voltage increase, which we can

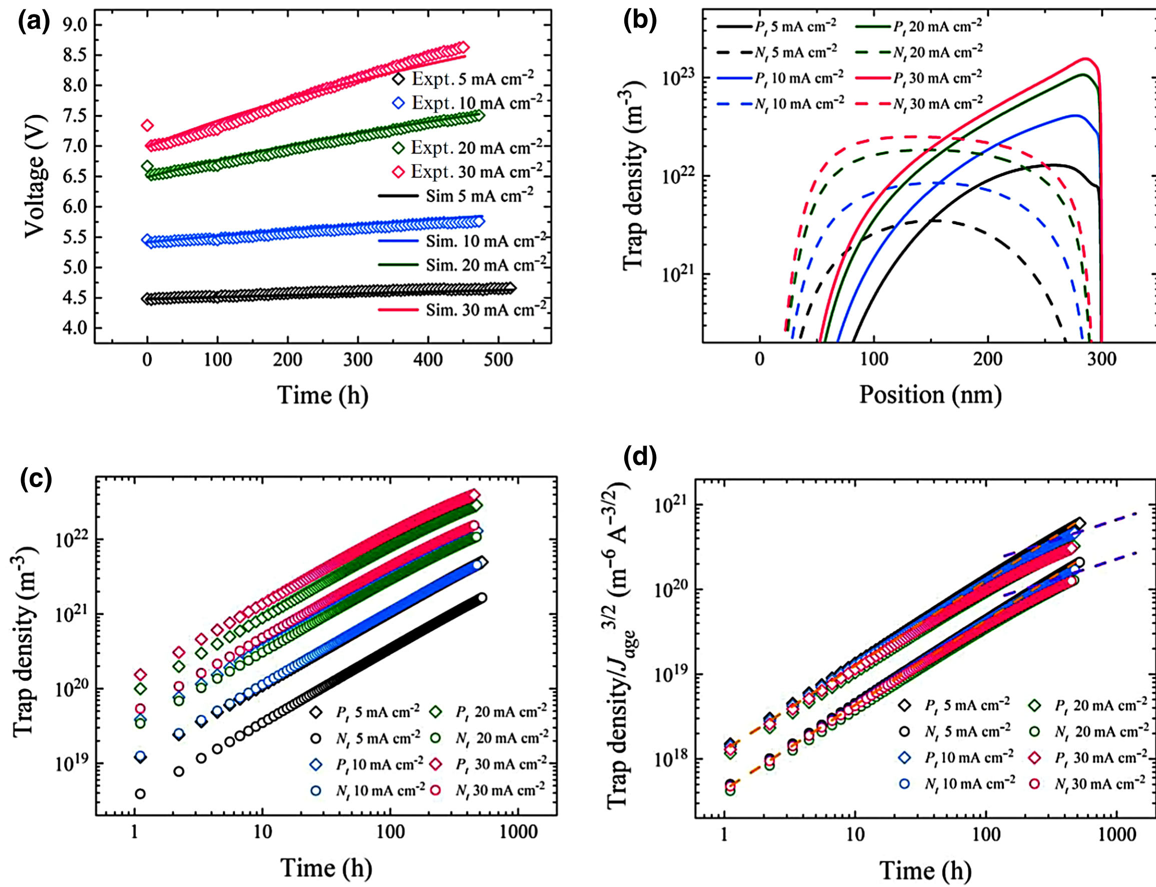

FIG. 2. Ageing behavior of CzDBA OLEDs. Ageing behavior of 300-nm CzDBA OLEDs modeled with the TPA mechanism. (a) Driving voltage versus time under constant current density, where the experiments (Expt.) are complimented by simulations (Sim.). (b) Trap density versus distance to the cathode in the device for all values of J_{age} (5–30 $\mathrm{mA\,cm^{-2}}$) at the end of the aging test. (c) Extracted hole (h) and electron (e) trap density versus aging time. (d) Trap density scales with ${J_{\mathrm{age}}}^{3/2}$. Dashed orange and violet lines have a slope of 1 and 0.5, respectively, as a guide to the eye. Note that the experimental time step is 10 s, but for readability several points are skipped between data points shown here.

do for each trap depth. The situation will then be such that deeper traps need a lower κ to fit the experiment, meaning that the lower the number of degradation traps generated, the deeper the degradation trap is. Consequently, *for different values of* κ, the simulated light output will move upwards with increasing trap depth. By considering both the voltage increase and the light output, combinations of the trap depth and κ can be found.

The modeling of the voltage over time can be seen in Fig. 2(a) for four different values of J_{age}, where we achieve a good fit with a degradation trap depth of 0.55 eV and $\kappa = 1.75 \times 10^{-28}\ \mathrm{m^3\,s^{-1}}$. The same combination of trap depth and κ describes the degradation of the 140-nm OLED, as seen in Figs. S3(a) and S3(b) within the Supplemental Material [59]. This is a strong indication that TPA is responsible for device degradation. Through kinetic Monte Carlo simulations on TADF multilayer OLEDs, Hausenstein *et al*. [41] reported an annihilation rate per site in the range 10^{-2}–1 as function of position in the emissive layer, which, in combination with a site density of $10^{27}\ \mathrm{m^{-3}}$, would translate into an interaction parameter in the 10^{-29}–$10^{-27}\ \mathrm{m^3\,s^{-1}}$ range, similar to what we find.

At the end of the degradation tests, the position-dependent trap profiles are plotted in Fig. 2(b), where the trap distribution can clearly be seen. The hole-trap density peaks near the anode, while electron traps are more homogenously distributed, with a slight increase in trap density towards the cathode at higher aging currents. The average trap density within these profiles versus time is shown in Fig. 2(c). The generated-trap density stays low, below $1 \times 10^{22}\ \mathrm{m^{-3}}$ at early times. It is known that such a low trap density does not impact on the J-V characteristics at room temperature [26]; consequently, we see an almost flat voltage curve at early times, as shown in Figs. 2(a) and S1 within the Supplemental Material [59]. Only when the trap density exceeds $1 \times 10^{22}\ \mathrm{m^{-3}}$, for example, around 30 h for $J_{\mathrm{age}} = 30\ \mathrm{mA\,cm^{-2}}$, does the voltage

rise start to become experimentally significant. In Fig. 2(d), we plot all created defects (both broken LETs and degradation traps) with their $J_{\mathrm{age}}{}^{3/2}$ scaling, which causes the curves for P_t and N_t to collapse into a single curve, consistent with the TPA mechanism [26,27]. Also consistent with TPA is the linear dependence on the stress time at early times, as indicated by the dashed orange line. The square-root dependence (dashed violet line) at longer aging times is not reached for most aging currents, except for the highest aging current of 30 mA cm^{-2} and only later during degradation, where the trap density starts to overtake the free-carrier density.

To rule out other possible degradation mechanisms, we test how the voltage will increase if traps are created via TTA or STA. As seen in Fig. 3, neither match the shape of the experimental voltage increase, plotted here for 30 mA cm^{-2}. Here, the increase of voltage is steep at the beginning and then saturates too strongly at later times, largely deviating from the experimental results. It should be noted that such a strong saturation is a universal consequence of the STA or TTA model, since trap formation through TTA or STA depends on the product of the emissive species, while, in the case of TPA, it depends only linearly on the triplet concentration. In a continuous cycle, the nonradiative SRH recombination from the created degradation traps will reduce the singlet density, S, and triplet density, T, which, in turn, slows the trap formation down. In STA and TTA, this affects both constituents of the process, whereas in TPA only the triplets are affected. The outcome is that, for STA and TTA, the voltage increase saturates too quickly compared to the experiment. These results furthermore confirm the dominance of TPA as the main mechanism of TADF OLED degradation.

As mentioned, we find the parameter κ governing the interaction between charge carriers and triplet excitons to be around 1.75×10^{-28} m^3 s^{-1} for every aging current density. To compare this number with the interaction parameter found previously for PLEDs, κ from this work needs to be multiplied by the effective triplet lifetime of 4.5 μs [44]. For PLEDs, we find a proportionality constant of trap formation of around 2×10^{-33} m^3, whereas the value for TADF is around 8×10^{-34} m^3. Remarkably, these two values are very close, differing only by a factor of 2.5, indicating that the intrinsic degradation mechanism, breaking of bonds by excited charge carries, is not different. With nearly equal interaction strength, it also follows why in a CzDBA OLED the voltage increase and trap formation are much slower compared to a SY PPV PLED (Fig. S1 within the Supplemental Material [59]). In PLEDs, triplet excitons have a lifetime of about 100 μs [30], resulting in a large build up of triplets in steady-state operation. In contrast, in CzDBA, the effective triplet lifetime is only around 4 μs due to efficient RISC. In CzDBA OLEDs, the build up of triplets under steady-state operation is thus much smaller and, consequently, with a similar interaction parameter the amount of interactions, and thus, the formed trap density, is much lower. This underlines the pivotal role of RISC in the context of OLED lifetimes.

D. Quantitative modeling of degraded OLEDs

With the degradation in time modeled, we can move back to the J-V and absolute-efficiency curves after degradation with a quantitative approach. The trap profiles for the 140-nm OLEDs are shown in Fig. S4(a) within the Supplemental Material [59]. For quantitative modeling, we can use these trap profiles as an input, to predict J-V and efficiency after degradation. Position-averaged values are

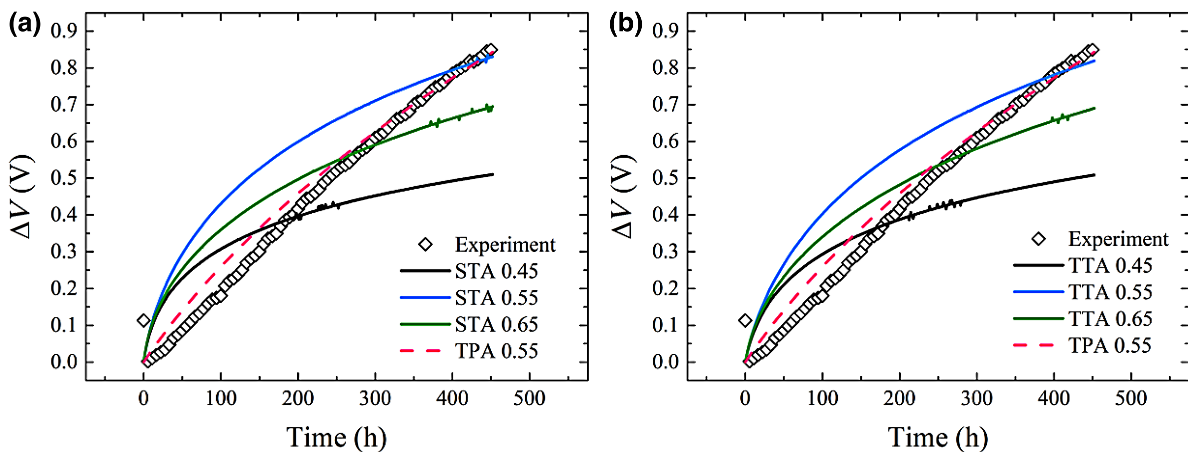

FIG. 3. Voltage increase over time during current stress. ΔV versus time for a 140-nm OLED aged at $J_{\mathrm{age}} = 30$ mA cm^{-2}. Lines show the simulated voltage increase predicted from trap formation based on (a) STA and (b) TTA. Colors correspond to different trap depths (in eV). Interaction coefficient for the different trap depths is kept constant at 6×10^{-26} m^3 s^{-1} for STA and 1.8×10^{-27} m^3 s^{-1} for TTA. Note that the experimental time step is 10 s, but for readability several points are skipped between the data points shown here. As a comparison, the results from the TPA model are shown as a dashed pink line.

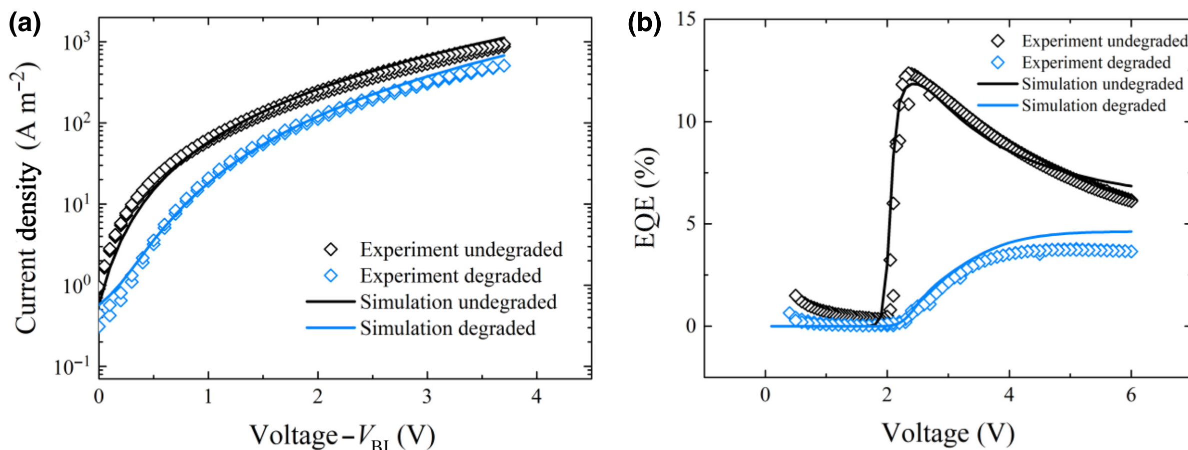

FIG. 4. Current and EQE versus voltage for pristine and degraded OLEDs. (a) J-V (corrected for V_{BI}) and (b) EQE of 140-nm (un)degraded OLEDs (symbols) complemented by simulations (lines) ($J_{age} = 20$ mA cm^{-2}). Position-dependent trap profiles are taken as input for the simulations here.

often considered in OLED modeling as an approximation, but the advantage of such a position-dependent approach is that it is ultimately more realistic. In thin emissive layers, neglecting the position dependence might be valid [60]; however, earlier modeling of undegraded CzDBA OLEDs with thicker emission zones revealed that neglecting the position dependence led to inconsistencies in the values of k_{TTA} with varying temperature [46]. As shown in Fig. 4, the resulting simulations are able to consistently describe the J-V and EQE-V characteristics after degradation well, considering these are predictions and not fits. We would like to underline the noticeable difference between undegraded and degraded samples in terms of roll-off, which depends strongly on the number of triplets in the active layer. The additional SRH recombination from the degradation traps and the breaking of LETs removes triplets, therefore, competing with other triplet decay channels, such as TTA, that are responsible for the roll-off [46]. As a result, the degraded efficiency curves will have less roll-off and look more like PLED efficiency curves instead, where roll-off is also absent due to the dark nature of triplet states. Figure S4(b) within the Supplemental Material [59] shows the effect of degradation traps on the recombination profile inside the device. We also plot the undegraded profile to show that the maximum of the recombination zone is pulled slightly towards the center of the device, as a consequence of the creation of hole and electron traps.

E. Lifetime enhancement with reduced TPA

Our numerical model can now quantitatively predict several scenarios that lead to a lifetime enhancement. The first strategy that is often mentioned is increasing the value of k_{RISC}, as this will lower the triplet population, and thus, the TPA interaction [61]. Figure 5(a) shows that increasing k_{RISC} from the standard value by a factor of 3 leads to an increase in T_{50} (time it takes to reach 50% of the initial luminance) of about 1.5 times, whereas lowering k_{RISC} indeed worsens the lifetime. Unfortunately, many variables go into the molecular design of TADF emitters. Enhancing k_{RISC} without affecting properties like charge transport is not straightforward, although promising efforts have been made through attaching multiple electron-donating units to a donor–acceptor-type TADF system [62]. As expected, the calculated lifetime is improved through the enhancement in k_{RISC}.

As reported before [21,23,51], controlling the distribution of triplets and carriers inside the active layer is another way to mitigate their interaction that leads to trap formation. The lifetime has the potential to be enhanced through broadening of the recombination zone. This allows us to formulate a rather straightforward strategy to achieve a higher lifetime, namely, to make a device with a thicker emissive layer, something that does not require additional molecular design. As a last point of discussion, we quantitatively address the influence of the active-layer thickness on the OLED lifetime. For this purpose, we consider the T_{80} lifetime at an initial luminescence of 1000 cd m^{-2}, which is the time it takes to reach 80% of the initial luminance. Using the experimentally obtained hole-only and electron-only parameters and $\kappa = 1.4 \times 10^{-28}$ m^3 s^{-1}, we predict the T_{80} values for CzDBA-layer thicknesses ranging from 50 to 300 nm. The theoretical curve for the TPA degradation mechanism is shown in Fig. 5(b) and the experimental T_{80} lifetime for different thicknesses is well matched. The fact that we see a lifetime variation with thickness in the first place proves that the degradation of our CzDBA OLEDs is an effect that comes from the bulk, as injection-related effects will not show a thickness-dependent lifetime [63]. The thick 300-nm OLED achieves a stability of 1050 h for T_{80}, which, for the lifetime of single-layer TADF OLEDs, exceeds many of the lifetimes

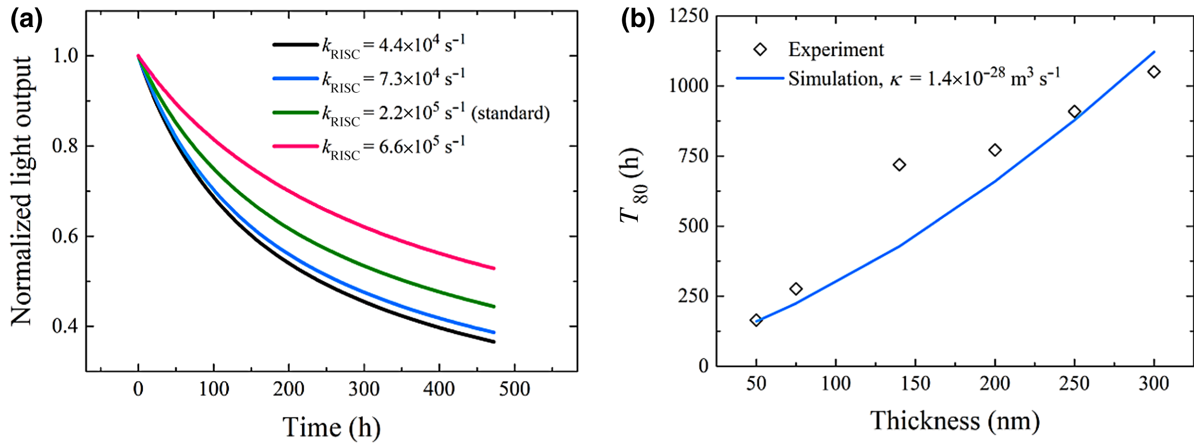

FIG. 5. Lifetime enhancement strategies. (a) Normalized light output versus time for different simulated values of k_{RISC}. Indication of "standard" means this value of k_{RISC} is used throughout the simulations. (b) T_{80} versus active-layer thickness for CzDBA OLEDs.

reported for multilayer OLEDs [38,40,44]. Our results correspond to a T_{95} of about 200 h, however, it is still an order of magnitude below that recently reported for a TADF OLED, namely, a T_{95} lifetime of 4500 h, with a multilayer architecture and a different emitter [64].

III. CONCLUSION

We quantitatively describe the degradation of OLEDs based on the TADF emitter CzDBA. We use a position-dependent model, where we incorporate the degradation-induced formation of both hole and electron traps by means of TPA, with the consideration of the disabling of emissive trap states. The model accurately describes the J-V and efficiency-voltage characteristics after degradation, as well as the voltage and light output versus time under current stress. Despite the observed aging behavior between PLEDs and TADF OLEDs, we demonstrate that they both exhibit the same degradation mechanism, resulting from TPA-dominated trap formation, in agreement with recent findings on multilayer TADF OLEDs [37]. Other mechanisms like TTA and STA fail to describe the degradation curves under current stress. Finally, we demonstrate that strategies which reduce the triplet concentration in the steady state, either by enhancing k_{RISC} or broadening the recombination zone, can significantly elongate the operation stability. Thick single-layer OLEDs with a broadened emission zone can reach a T_{80} of 1050 h at an initial luminescence of 1000 cd m^{-2}.

IV. METHODS

A. Device fabrication

ITO substrates are treated in a cleanroom environment with soap and subsequently sonicated in acetone and isopropanol for 10 min each. Afterwards, a hole-injection layer of poly(3,4-ethylenedioxythiophene):polystyrene sulfonate (40 nm) (Heraeus Clevios 4083) is spin-coated from an aqueous solution and annealed at 140 °C for 10 min. Next, several layers are evaporated by thermal deposition, which we show in the following structure: "material name" ("thickness," "rate of evaporation"). The layers are MoO_3 (7 nm, 0.12–0.15 Å s^{-1}), C_{60} (3 nm, 0.12 Å s^{-1}), the CzDBA active layer (various thicknesses described in the main text, 0.25–0.3 Å s^{-1}), and 2,2′,2″-(1,3,5-Benzinetriyl)-tris(1-phenyl-1-H-benzimidazole) (4 nm, 0.12 Å s^{-1}). To complete the OLED, aluminum (100 nm) is evaporated. All evaporations are done in a glovebox environment with oxygen and water values below 0.1 ppm and at a pressure of around $3 \times 10^{--6}$ mbar.

B. Device characterization

J-V measurements are carried out with a Keithley 2400 source meter, while simultaneously the photocurrent-voltage measurements are carried out with a Keithley 6514 system electrometer. The EQE measurements are done using a calibrated Si photodiode with an area larger than that of the emitting pixel. All device characterization is done in an inert environment (O_2 and H_2O values below 0.1 ppm). The lifetime setup is home-built and consists of a voltage source, photodiode, and a LabView program for controlling the hardware and reading out the voltage and light output data. All lifetime data are collected on a pixel with an area size of 8.1×10^{-6} m^2. The lifetime measurements are done in the dark and in a controlled glovebox environment with O_2 and H_2O values below 0.1 ppm.

C. Simulation

Our drift-diffusion simulations use an iterative scheme to calculate n and p with a tolerance of 1×10^{-6} on an active layer that contains 1000 points on an exponential symmetric grid normalized to unity. The simulation

parameters for an undegraded device are given in Tables S1 and S2 within the Supplemental Material [59]. Further notable input parameters include the electrical band gap of CzDBA, which is determined from OLED data to be 2.8 eV, and the relative permittivity, which is set to 3. Both current and charge-carrier density values converge if their values between loops vary less than the said tolerance. For stability, the iterative loop is usually repeated 5 times, and the calculated mobility values are averaged over all iterative loops. Once convergence is reached, the SRH and Langevin recombination rate are combined into the generation rate to take the effect of LETs into account. The singlet and triplet populations are then calculated according to formulas documented in Ref. [46], taking the effect of TTA into account. The simulation of the degradation characteristics over time uses the same procedure as that outlined above, but it is done for each time step, which is generally kept at 4000 s. As stated in the manuscript, at the end of each time loop, the formed degradation traps and how many LETs are broken are calculated according to Eq. (2).

[1] Y. Zhang, J. Lee, and S. R. Forrest, Tenfold increase in the lifetime of blue phosphorescent organic light-emitting diodes, Nat. Commun. **5**, 5008 (2014).

[2] D. Wang, C. Cheng, T. Tsuboi, and Q. Zhang, Degradation mechanisms in blue organic light-emitting diodes, CCS Chem. **2**, 1278 (2020).

[3] D. Zhang, M. Cai, Y. Zhang, D. Zhang, and L. Duan, Sterically shielded blue thermally activated delayed fluorescence emitters with improved efficiency and stability, Mater. Horiz. **3**, 145 (2016).

[4] X. Cai and S.-J. Su, Marching toward highly efficient, pure-blue, and stable thermally activated delayed fluorescent organic light-emitting diodes, Adv. Funct. Mater. **28**, 1802558 (2018).

[5] K. Goushi, K. Yoshida, K. Sato, and C. Adachi, Organic light-emitting diodes employing efficient reverse intersystem crossing for triplet-to-singlet state conversion, Nat. Photonics **6**, 253 (2012).

[6] H. Uoyama, K. Goushi, K. Shizu, H. Nomura, and C. Adachi, Highly efficient organic light-emitting diodes from delayed fluorescence, Nature **492**, 234 (2012).

[7] J. H. Kim, J. H. Yun, and J. Y. Lee, Recent progress of highly efficient red and near-infrared thermally activated delayed fluorescent emitters, Adv. Opt. Mater. **6**, 1800255 (2018).

[8] M. Y. Wong and E. Zysman-Colman, Purely organic thermally activated delayed fluorescence materials for organic light-emitting diodes, Adv. Mater. **29**, 1605444 (2017).

[9] Z. Yang, Z. Mao, Z. Xie, Y. Zhang, S. Liu, J. Zhao, J. Xu, Z. Chi, and M. P. Aldred, Recent advances in organic thermally activated delayed fluorescence materials, Chem. Soc. Rev. **46**, 915 (2017).

[10] D. H. Ahn, S. W. Kim, H. Lee, I. J. Ko, D. Karthik, J. Y. Lee, and J. H. Kwon, Highly efficient blue thermally activated delayed fluorescence emitters based on symmetrical and rigid oxygen-bridged boron acceptors, Nat. Photonics **13**, 540 (2019).

[11] Y.-L. Zhang, Q. Ran, Q. Wang, Y. Liu, C. Hänisch, S. Reineke, J. Fan, and L.-S. Liao, High-efficiency red organic light-emitting diodes with external quantum efficiency close to 30% based on a novel thermally activated delayed fluorescence emitter, Adv. Mater. **31**, 1902368 (2019).

[12] S.-J. Zou, F.-M. Xie, M. Xie, Y.-Q. Li, T. Cheng, X.-H. Zhang, C.-S. Lee, and J.-X. Tang, High-performance nondoped blue delayed fluorescence organic light-emitting diodes featuring low driving voltage and high brightness, Adv. Sci. **7**, 1902508 (2020).

[13] S. S. Swayamprabha, D. K. Dubey, Shahnawaz, A. K. Y. Rohit, M. R. Nagar, A. Sharma, F.-C. Tung, and J.-H. Jou, Approaches for long lifetime organic light emitting diodes, Adv. Sci. **8**, 2002254 (2021).

[14] A. S. D. Sandanayaka, T. Matsushima, and C. Adachi, Degradation mechanisms of organic light-emitting diodes based on thermally activated delayed fluorescence molecules, J. Phys. Chem. C **11**, 23845 (2015).

[15] T.-H. Han, W. Song, and T.-W. Lee, Elucidating the crucial role of hole injection layer in degradation of organic light-emitting diodes, ACS Appl. Mater. Interfaces **7**, 3117 (2015).

[16] W. S. Jun, Y. Lee, T. Kim, Y. Lee, and H. Jeong, Comprehensive understanding of degradation mechanism of high efficiency blue organic light-emitting diodes at the interface by hole and electron transport layer, Org. Electron. **57**, 158 (2018).

[17] R. Meerheim, S. Scholz, S. Olthof, G. Schwartz, S. Reineke, K. Walzer, and K. Leo, Influence of charge balance and exciton distribution on efficiency and lifetime of phosphorescent organic light-emitting devices, J. Appl. Phys. **104**, 014510 (2008).

[18] H. Fukagawa, T. Shimizu, H. Kawano, S. Yui, T. Shinnai, A. Iwai, K. Tsuchiya, and T. Yamamoto, Novel hole-transporting materials with high triplet energy for highly efficient and stable organic light-emitting diodes, J. Phys. Chem. C **120**, 18748 (2016).

[19] F. So and D. Kondakov, Degradation mechanisms in small-molecule and polymer organic light-emitting diodes, Adv. Mater. **22**, 3762 (2010).

[20] S.-G. Ihn, N. Lee, S. O. Jeon, M. Sim, H. Kang, Y. Jung, D. H. Huh, Y. M. Son, S. Y. Lee, M. Numata, *et al.*, An alternative host material for long-lifespan blue organic light-emitting diodes using thermally activated delayed fluorescence, Adv. Sci. **4**, 1600502 (2017).

[21] L.-S. Cui, S.-B. Ruan, F. Bencheikh, R. Nagata, L. Zhang, K. Inada, H. Nakanotani, L.-S. Liao, and C. Adachi, Long-lived efficient delayed fluorescence organic light-emitting diodes using *n*-type hosts, Nat. Commun. **8**, 2250 (2017).

[22] L.-S. Cui, Y.-M. Xie, Y.-K. Wang, C. Zhong, Y.-L. Deng, X.-Y. Liu, Z.-Q. Jiang, and L.-S. Liao, Pure hydrocarbon hosts for ≈100% exciton harvesting in both phosphorescent and fluorescent light-emitting devices, Adv. Mater. **27**, 4213 (2015).

[23] H. Nakanotani, K. Masui, J. Nishide, T. Shibata, and C. Adachi, Promising operational stability of high-efficiency organic light-emitting diodes based on thermally activated delayed fluorescence, Sci. Rep. **3**, 2127 (2013).

[24] Q. Niu, G. A. H. Wetzelaer, P. W. M. Blom, and N. I. Crăciun, Modeling of electrical characteristics of degraded polymer light-emitting diodes, Adv. Electron. Mater. **2**, 1600103 (2016).

[25] G. C. M. Silvestre, M. T. Johnson, A. Giraldo, and J. M. Shannon, Light degradation and voltage drift in polymer light-emitting diodes, Appl. Phys. Lett. **78**, 1619 (2001).

[26] Q. Niu, R. Rohloff, G. A. H. Wetzelaer, P. W. M. Blom, and N. I. Crăciun, Hole trap formation in polymer light-emitting diodes under current stress, Nat. Mater. **17**, 557 (2018).

[27] B. van der Zee, S. Paulus, R.-Q. Png, P. K. H. Ho, L.-L. Chua, G.-J. A. H. Wetzelaer, and P. W. M. Blom, Role of singlet and triplet excitons on the electrical stability of polymer light-emitting diodes, Adv. Electron. Mater. **6**, 2000367 (2020).

[28] O. Pekkola, A. Gassmann, F. Etzold, F. Laquai, and H. von Seggern, Influence of triplet excitons on the lifetime of polymer-based organic light emitting diodes, Phys. Status Solidi A **211**, 2035 (2014).

[29] I. Rörich, A.-K. Schönbein, D. K. Mangalore, A. H. Ribeiro, C. Kasparek, C. Bauer, N. I. Crăciun, P. W. M. Blom, and C. Ramanan, Temperature dependence of the photo- and electroluminescence of poly(*p*-phenylene vinylene) based polymers, J. Mater. Chem. C **6**, 10569 (2018).

[30] S. Dhoot, D. S. Ginger, D. Beljonne, Z. Shuai, and N. C. Greenham, Triplet formation and decay in conjugated polymer devices, Chem. Phys. Lett. **360**, 195 (2002).

[31] D. K. Tsang, T. Matsushima, and C. Adachi, Operational stability enhancement in organic light-emitting diodes with ultrathin Liq interlayers, Sci. Rep. **6**, 22463 (2016).

[32] S. Kothavale, W. J. Chung, and J. Y. Lee, High efficiency and long lifetime orange-red thermally activated delayed fluorescent organic light emitting diodes by donor and acceptor engineering, J. Mater. Chem. C **9**, 528 (2021).

[33] Y. J. Cho, S. K. Jeon, and J. Y. Lee, Molecular engineering of high efficiency and long lifetime blue thermally activated delayed fluorescent emitters for vacuum and solution processed organic light-emitting diodes, Adv. Opt. Mater. **4**, 688 (2016).

[34] M. Kim, S. K. Jeon, S.-H. Hwang, and J. Y. Lee, Stable blue thermally activated delayed fluorescent organic light-emitting diodes with three times longer lifetime than phosphorescent organic light-emitting diodes, Adv. Mater. **27**, 2515 (2015).

[35] S. Scholz, D. Y. Kondakov, B. Lüssem, and K. Leo, Degradation mechanisms and reactions in organic light-emitting devices, Chem. Rev. **115**, 8449 (2015).

[36] J. Lee, C. Jeong, T. Batagoda, C. Coburn, M. E. Thompson, and S. R. Forrest, Hot excited state management for long-lived blue phosphorescent organic light-emitting diodes, Nat. Commun. **8**, 15566 (2017).

[37] M. Tanaka, R. Nagata, H. Nakanotani, and C. Adachi, Understanding degradation of organic light-emitting diodes from magnetic field effects, Commun. Mater. **1**, 18 (2020).

[38] C.-Y. Chan, M. Tanaka, H. Nakanotani, and C. Adachi, Efficient and stable sky-blue delayed fluorescence organic light-emitting diodes with CIE_y below 0.4, Nat. Commun. **9**, 5036 (2018).

[39] M. Hasan, S. Saggar, A. Shukla, F. Bencheikh, J. Sobus, S. K. M. McGregor, C. Adachi, S.-C. Lo, and E. B. Namdas, Probing polaron-induced exciton quenching in TADF based organic light-emitting diodes, Nat. Commun. **13**, 254 (2022).

[40] M. Tanaka, H. Noda, H. Nakanotani, and C. Adachi, Effect of carrier balance on device degradation of organic light-emitting diodes based on thermally activated delayed fluorescence emitters, Adv. Electron. Mater. **5**, 1800708 (2019).

[41] C. Hauenstein, S. Gottardi, E. Torun, R. Coehoorn, and H. van Eersel, Identification of OLED degradation scenarios by kinetic Monte Carlo simulations of lifetime experiments, Front. Chem. **9**, 823210 (2022).

[42] S. Schmidbauer, A. Hohenleutner, and B. König, Chemical degradation in organic light-emitting devices: mechanisms and implications for the design of new Materials, Adv. Mater. **25**, 2114 (2013).

[43] A. Gassmann, S. V. Yampolskii, A. Klein, K. Albe, N. Vilbrandt, O. Pekkola, Y. A. Genenko, M. Rehahn, and H. von Seggern, Study of electrical fatigue by defect engineering in organic light-emitting diodes, Mater. Sci. Eng., B **192**, 26 (2015).

[44] T.-L. Wu, M.-J. Huang, C.-C. Lin, P.-Y. Huang, T.-Y. Chou, R.-W. Chen-Cheng, H.-W. Lin, R.-S. Liu, and C.-H. Cheng, Diboron compound-based organic light-emitting diodes with high efficiency and reduced efficiency roll-off, Nat. Photonics **12**, 235 (2018).

[45] B. van der Zee, Y. Li, G.-J. A. H. Wetzelaer, and P. W. M. Blom, Origin of the efficiency roll-off in single-layer organic light-emitting diodes based on thermally activated delayed fluorescence, Adv. Opt. Mater. **9**, 2100249 (2021).

[46] B. van der Zee, Y. Li, G.-J. A. H. Wetzelaer, and P. W. M. Blom, Numerical device model for organic light-emitting diodes based on thermally activated delayed fluorescence, Adv. Electron. Mater. **8**, 2101261 (2021).

[47] D. Y. Kondakov, W. C. Lenhart, and W. F. Nichols, Operational degradation of organic light-emitting diodes: Mechanism and identification of chemical products, J. Appl. Phys. **101**, 024512 (2007).

[48] N. B. Kotadiya, H. Lu, A. Mondal, Y. Ie, D. Andrienko, P. W. M. Blom, and G.-J. A. H. Wetzelaer, Universal strategy for ohmic hole injection into organic semiconductors with high ionization energies, Nat. Mater. **17**, 329 (2018).

[49] W. Liu, N. B. Kotadiya, P. W. M. Blom, G.-J. A. H. Wetzelaer, and D. Andrienko, Molecular origin of balanced bipolar transport in neat layers of the emitter CzDBA, Adv. Mater. Technol. **6**, 2000120 (2021).

[50] N. B. Kotadiya, A. Mondal, P. W. M. Blom, D. Adrienko, and G. A. H. Wetzelaer, A window to trap-free charge transport in organic semiconducting thin films, Nat. Mater. **18**, 1182 (2019).

[51] N. B. Kotadiya, P. W. M. Blom, and G. A. H. Wetzelaer, Efficient and stable single-layer organic light-emitting diodes based on thermally activated delayed fluorescence, Nat. Photonics **13**, 765 (2019).

[52] W. F. Pasveer, J. Cottaar, C. Tanase, R. Coehoorn, P. A. Bobbert, P. W. M. Blom, D. M. de Leeuw, and M. A. J. Michels, Unified Description of Charge-Carrier Mobilities

in Disordered Semiconducting Polymers, Phys. Rev. Lett. **94**, 206601 (2005).

[53] D. Abbaszadeh, A. Kunz, G. A. H. Wetzelaer, J. J. Michels, N. I. Crăciun, K. Koynov, I. Lieberwirth, and P. W. M. Blom, Elimination of charge carrier trapping in diluted semiconductors, Nat. Mater. **15**, 628 (2016).

[54] P. W. M. Blom and M. C. J. M. Vissenberg, Charge transport in poly(*p*-phenylene vinylene) light-emitting diodes, Mater. Sci. Eng., R **27**, 53 (2000).

[55] H. T. Nicolai, M. Kuik, G. A. H. Wetzelaer, B. de Boer, C. Campbell, C. Risko, J. L. Brédas, and P. W. M. Blom, Unification of trap-limited electron transport in semiconducting polymers, Nat. Mater. **11**, 882 (2012).

[56] M. Kuik, L. J. A. Koster, A. G. Dijkstra, G. A. H. Wetzelaer, and P. W. M. Blom, Non-radiative recombination losses in polymer light-emitting diodes, Org. Electron. **13**, 969 (2012).

[57] M. K. Etherington, N. A. Kukhta, H. F. Higginbotham, A. Danos, A. N. Bismillah, D. R. Graves, P. R. McGonigal, N. Haase, A. Morherr, A. S. Batsanov, *et al.*, Persistent dimer emission in thermally activated delayed fluorescence materials, J. Phys. Chem. C **123**, 11109 (2019).

[58] E. Cho, M. Hong, V. Coropceanu, and J. L. Brédas, The role of intermolecular interactions on the performance of organic thermally activated delayed fluorescence (TADF) materials, Adv. Opt. Mater. **9**, 2002135 (2021).

[59] See the Supplemental Material at http://link.aps.org/supplemental/10.1103/PhysRevApplied.18.064002 contains a comparison between the voltage increase of a TADF OLED and a PLED. Furthermore, it shows how a unique set of fitting parameters can be determined by considering the voltage increase as well as the light decrease during degradation, and that these parameters can be used for 140-nm thick devices. The final graphs concern the position dependence of several quantities.

[60] M. A. Baldo, C. Adachi, and S. R. Forrest, Transient analysis of organic electrophosphorescence. II. Transient analysis of triplet-triplet annihilation, Phys. Rev. B **62**, 10967 (2000).

[61] H. J. Lee, H. L. Lee, S. H. Han, and J. Y. Lee, Novel secondary acceptor based molecular design for superb lifetime in thermally activated delayed fluorescent organic light-emitting diodes through high bond energy and fast up-conversion, Chem. Eng. J. **427**, 130988 (2022).

[62] H. Noda, H. Nakanotani, and C. Adachi, Excited state engineering for efficient reverse intersystem crossing, Sci. Adv. **4**, 6 (2018).

[63] I. D. Parker, Y. Cao, and C. Y. Yang, Lifetime and degradation effects in polymer light-emitting diodes, J. Appl. Phys. **85**, 2441 (1999).

[64] R. M. Ciarnáin, H. W. Mo, K. Nagayoshi, H. Fujimoto, K. Harada, R. Gehlhaar, T. H. Ke, P. Heremans, and C. Adachi, Thermally activated delayed fluorescence green OLED with 4500 h lifetime and 20% external quantum efficiency by optimizing the emission zone using a single-emission spectrum technique, Adv. Mater. **34**, 2201409 (2022).

[65] K. Thakur, B. van der Zee, G.-J. A. H. Wetzelaer, C. Ramanan, and P. W. M. Blom, Quantifying exciton annihilation effects in thermally activated delayed fluorescence materials, Adv. Opt. Mater. **10**, 2101784 (2021).